Optimization strategies in measurement based quantum computation

Giulia Ferrini, Jonathan Roslund, Francesco Arzani, Yin Cai, Claude Fabre, Nicolas Treps

Optimization strategies in measurement based quantum computation

G. Ferrini, J. Roslund, F. Arzani, Y. Cai, C. Fabre and N. Treps
Laboratoire Kastler Brossel, UPMC Univ. Paris 6,
ENS, CNRS; 4 place Jussieu, 75252 Paris, France
(Dated: July 20, 2014)

This work introduces optimization strategies to continuous variable measurement based quantum computation (MBQC) at different levels. We provide a recipe for mitigating the effects of finite squeezing, which affect the production of cluster states and the result of a traditional MBQC. These strategies are readily implementable by several experimental groups. Furthermore, a more general scheme for MBQC is introduced that does not necessarily rely on the use of ancillary cluster states to achieve its aim, but rather on the detection of a resource state in a suitable mode basis followed by digital post-processing. A recipe is provided to optimize the adjustable parameters that are employed within this framework.

PACS numbers:

Continuous Variable (CV) quantum computing in the measurement based approach [1, 2] has gained significant interest following recent experiments in which large cluster states have been constructed with time [3] or frequency [4] encoding. The ability to perform a quantum computation (QC) on a resource state that is consumed in time opens the possibility of scaling the computation to large mode numbers. One of the difficulties associated with CV measurement based quantum computing (MBQC) is that finite squeezing engenders errors that propagate through the computation and contribute extra noise to the result [5, 6]. Recently, however, a fault tolerant CV MBQC protocol was proposed [7] that utilizes extra ancillary modes and necessitates the squeezing of each input mode to be above a finite, albeit demanding, threshold. This result is encouraging and supports the positive outlooks for CV MBQC. However, a need still exists for QC protocols that minimize errors as much as possible for a given degree of squeezing and do so without introducing additional resources.

The objective of this Letter is twofold. First, we provide an optimization strategy that diminishes errors of a quantum computation arising from finite squeezing in the traditional MBQC approach. In particular, if the squeezing degree is not equivalent for all of the input modes, this approach optimally redistributes the available correlations among the transformed modes. The ability to employ optimization strategies is shown to result from tunable degrees of freedom contained within the unitary matrix that fabricates cluster states from a set of squeezed states [8–12]. Second, a new approach to MBQC is proposed that is distinct from the traditional one premised upon the use of cluster states. This scheme is software-based and utilizes post-processing following a measurement as a means to discover the most suitable basis in which to express the QC result. Thus, the method directly targets a desired result while also incorporating the possibility of minimizing extra noise. Both objectives are directly related to the task of optimizing a Gaussian MBQC given a set of finite resources.

We begin by carefully defining the objects to be optimized. Consider a general linear transformation, corresponding to a specific unitary matrix U, which acts on an initial set of squeezed modes $\vec{a}^{\,\mathrm{squ}} = (\hat{a}_1^{\mathrm{squ}}, ..., \hat{a}_N^{\mathrm{squ}})$:

$$\vec{a}\,' = U\vec{a}^{\,\mathrm{squ}}. \tag{1}$$

A given task, such as the creation of cluster states or the execution of a QC, is accomplished through judicious selection of the U matrix. This matrix is not unique, however, and several internal degrees of freedom may be exploited to minimize errors associated with the task.

As an example, in the case of cluster state creation with finitely squeezed inputs, U may be chosen so as to minimize the mean of the nullifier variances:

$$f_1 = \frac{1}{N}\sum_{i=1}^{N} \Delta^2 \delta_i \tag{2}$$

where $\left\{\Delta^2 \hat{\delta}_i\right\}$ are the nullifiers $\hat{\delta}_i \equiv \left(\hat{p}_i^C - \sum_l V_{il}\hat{x}_l^C\right)$, V is the adjacency matrix of the cluster state [5, 6]. This choice of function f_1 is not unique, and other analogous functions may be defined [31].

One may also consider that the transformation (1) is applied to an array of squeezed modes in which one of the input modes $\hat{a}_{\mathrm{in}}$ is to be processed by a Gaussian QC (in this situation, the input mode is prepended to the squeezed array, i.e., $\vec{a}^{\,\mathrm{squ}} \rightarrow (\hat{a}_{\mathrm{in}}, \vec{a}^{\,\mathrm{squ}})$). MBQC relies on the measurement of all the system modes (e.g., of the $\hat{p}$ quadrature) except for the last one (for simplicity, we restrict our attention to single mode operations). All of these measurements may be performed simultaneously without harming the determinism of the operation [5, 6]. The output mode (i.e., the unmeasured mode) is then expressible as a function of the input mode quadratures $\hat{p}_{\mathrm{in}}$ and $\hat{x}_{\mathrm{in}}$, the individual measurement results p_i', and the squeezed quadratures $\hat{p}_i^{\mathrm{squ}}$ of the input modes (i.e. it is possible to eliminate the contribution of anti-squeezed

quadratures as outlined in [13]):

$$\hat{x}_{\rm out} \equiv \hat{x}'_N = \sum_{i=1}^{N} c_i \hat{p}_i^{\rm squ} + j\hat{p}_{\rm in} + k\hat{x}_{\rm in} + \sum_{i=1}^{N-1} l_{xi} p'_i \quad (3)$$

$$\hat{p}_{\rm out} \equiv \hat{p}'_N = \sum_{i=1}^{N} b_i \hat{p}_i^{\rm squ} + d\hat{p}_{\rm in} + e\hat{x}_{\rm in} + \sum_{i=1}^{N-1} l_{pi} p'_i. \quad (4)$$

The coefficients $\{b_i\}, \{c_i\}, e, k, j, d,\ l_{p_i}$, and l_{xi} depend upon the specific transformation U that is applied to the input modes according to Eq.(1). The terms $\sum_{i=1}^{N-1} l_{x,p_i} p'_i$ are linear functions of the measurement outcomes that, although they may be corrected for, do not affect the symplectic structure of the input-output transformation [5, 6]. The output mode of Eqs.(3),(4) encodes the result of the QC, and its measurement (which can be simultaneous with the others) provides the result. One can then optimize U by minimizing f_2, such that the output of the quantum computation is the desired one:

$$f_2 = (|d - d_{\rm res}| + |e - e_{\rm res}| + |j - j_{\rm res}| + |k - k_{\rm res}|)/4, \quad (5)$$

where $e_{\rm res}, k_{\rm res}, j_{\rm res}, d_{\rm res}$ are coefficients of the desired result. Furthermore, it is also possible to reduce the excess noise incurred by finite squeezing by minimizing [32]

$$f_3 = \Delta^2\left(\sum_{i=1}^{N} c_i \hat{p}_i^{\rm squ}\right) + \Delta^2\left(\sum_{i=1}^{N} b_i \hat{p}_i^{\rm squ}\right) \equiv \Delta^2 \hat{x}_{\rm extra} + \Delta^2 \hat{p}_{\rm extra}. \quad (6)$$

In what follows, we show that these optimizations may be applied in various physical contexts, including traditional MBQC, as well as in more general approaches.

Optimization of cluster states. All of the possible matrices U_V that yield a V-graph cluster state from input squeezed modes (as defined by Eq.(1)) may be derived by generalizing the recipe of Ref. [8] (see [13] for details):

$$U_V(\vec{\theta}) = (1 + iV)(V^2 + I)^{-1/2} \mathcal{O}(\vec{\theta}), \quad (7)$$

where $\mathcal{O}(\vec{\theta})$ is any real orthogonal matrix ($\mathcal{O}(\vec{\theta})\mathcal{O}(\vec{\theta})^T = \mathcal{I}$) and is parameterized by $N(N-1)/2$ degrees of freedom $\vec{\theta}$ (e.g. Euler or Tait-Bryan angles). The matrix $\mathcal{O}(\vec{\theta})$ may be freely chosen to mitigate the effects of finite squeezing on cluster state preparation and MBQC. Selection of an optimal matrix is achieved by employing evolutionary strategies [14], which are particularly suitable for high-dimensional parameter searches. In practice, we search for a $\vec{\theta}$ that minimizes a fitness function, such as the ones previously described. Having discovered an optimal orthogonal matrix, the unitary matrix implementing the desired cluster state is fully specified.

If the squeezing levels for the input modes are uniform, all of the unitaries described by Eq.(7) are equivalent. For nonuniform squeezing levels, however, one may search for a unitary matrix U_V that redistributes the available squeezing among the modes in a manner that optimizes some desired property, e.g., f_1 in Eq.(2) [33]. As an example, we consider the fabrication of a 4-mode linear cluster state. The input modes are assumed to possess realistic squeezing levels, such as those seen in the four-mode multimode state of Ref. [15]. Specifically, the squeezed quadrature variances relative to shot noise (SN) level are taken as -7dB, -6dB, -4dB, and 0dB. The use of these modes to fashion a cluster state from the U_V defined in Ref.[9] yields the nullifier variances reported in Table I (with the convention $\Delta^2_{vac} = 1$), where the final nullifier lies at the SN level. Yet, by optimizing the angles $\vec{\theta}$ in Eq.(7) to minimize f_1, all of the nullifier variances are lowered below the SN level and f_1 is reduced by 23%. Consequently, the optimization successfully reduces the residual error induced by finite squeezing. Importantly, this procedure may be applied to a cluster state of arbitrary dimension as well as to the case of non-pure states [13].

	Nullifier variances $\{\frac{\Delta^2\delta_i}{\Delta^2\delta_{i0}}\}$	f_1
Network U_V from Ref.[9]	$\{0.20, 0.50, 0.24, 1.0\}$	1.16
Optimized network $U_V^{\rm best}$	{0.41,0.28,0.29,0.51}	0.89
Optimized matrix $U_{\rm MHD}^{\rm best}$	{0.23,0.48,0.21,0.70}	0.97

TABLE I: Comparison of nullifier variances for a 4-node linear cluster state with and without optimization of the unitary transformation U. $\Delta^2\delta_{i0}$ are the shot noise (SN) levels, which are defined as the nullifier variances for vacua inputs.

MBQC error reduction. The ability to minimize cluster state nullifiers may be directly translated to the task of reducing errors of a MBQC in the cluster-based approach [8]. For this application, the unitary in Eq.(1) results from the product of three matrices: the unitary U_V constructing the cluster from the input squeezed modes, the beamsplitter interaction between the input state and a single mode of the cluster, and a proper diagonal matrix specifying each mode's measurement quadrature:

$$U = U_{\rm comp} = D_{\rm meas} U_{\rm BS} U_V(\vec{\theta}). \quad (8)$$

This choice of unitary matrix U leads to a value of zero for the f_2 function of Eq.(5). Importantly, the excess noise remaining in Eqs.(3),(4), expressed by f_3, may be recast in terms of the cluster nullifiers [8, 13, 16].

As an example, we consider a Fourier transformation of the input state, i.e. $\begin{pmatrix} \hat{x}_{\rm out} \\ \hat{p}_{\rm out} \end{pmatrix} = \begin{pmatrix} 0 & -1 \\ 1 & 0 \end{pmatrix} \begin{pmatrix} \hat{x}_{\rm in} \\ \hat{p}_{\rm in} \end{pmatrix} = \begin{pmatrix} -\hat{p}_{\rm in} \\ \hat{x}_{\rm in} \end{pmatrix}$. The measurement matrix $D_{\rm meas}$ along with the U_V necessary to implement this QC by a three-mode cluster state are reported in Ref. [17] (see also [13]). The calculation of the output mode containing the computa-

	$\Delta^2\hat{x}_{\rm extra}$	$\Delta^2\hat{p}_{\rm extra}$	f_2	f_3
$U_{\rm comp}$ from Ref.[17]	1.20	0.48	0	1.70
Optimized $U_{\rm comp}^{\rm best}$	0.60	0.50	0	1.10
Optimized matrix $U_{\rm MHD}^{\rm best}$	0.25	0.18	10^{-16}	0.43

TABLE II: Comparison of a QC's excess noise with and without optimization of the unitary transformation U.

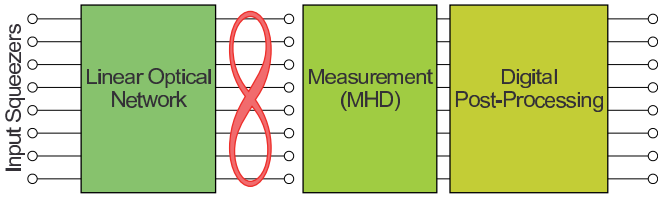

FIG. 1: Schematic for the construction of quantum operations with a multimode homodyne detector (MHD) followed by digital post-processing.

tion result follows the lines of Refs. [8, 18] and yields [13]

$$\begin{aligned}\hat{x}_{\rm out} &= \hat{x}'_3 = -\hat{p}_{\rm in} + p'_2 - \sqrt{2}p'_1 - \hat{\delta}_2 \\ \hat{p}_{\rm out} &= \hat{p}'_3 = \hat{x}_{\rm in} - \sqrt{2}p'_{\rm in} - \hat{\delta}_1 + \hat{\delta}_3,\end{aligned} \tag{9}$$

where $\hat{\delta}_i$ are the previously defined nullifiers depending upon the chosen realization of $U_V(\vec{\theta})$. By optimizing $\mathcal{O}(\vec{\theta})$, we have already shown that the nullifier variances are minimized, thereby reducing the error of the QC.

As a demonstration of the optimization scheme in the context of MBQC, the squeezing distribution of Ref. [15] is again considered where the fourth (minimally squeezed) mode serves as the input mode. In the absence of any optimization (i.e., $\mathcal{O}(\vec{\theta}) = \mathcal{I}$ and $U_V(\vec{\theta})$ is given in Ref. [17]), the excess noise quadratures $\Delta^2\hat{x}_{\rm extra} = \Delta^2\hat{\delta}_2$ and $\Delta^2\hat{p}_{\rm extra} = \Delta^2(-\hat{\delta}_1+\hat{\delta}_3)$ in Eq.(9) are detailed in Table II [34]. By optimizing f_3 over $\vec{\theta}$, it is possible to suppress the total noise by $\sim 35\%$ (see Table II). It is important to note that the obtained noise reduction is specific to the distribution of input squeezing values. Nonetheless, these results readily generalize to more complicated clusters, including the support of multimode operations.

To conclude this section, we stress that any experimental group investigating MBQC on cluster states generated by a linear optical network U_V may employ these optimization strategies to mitigate errors associated with finite and nonuniform squeezing of the input modes.

Directly synthesized cluster states and MBQC. A tangible optical network is actually unnecessary for collecting statistics corresponding to detection of each cluster mode's quadrature or the end result of a QC. A general experimental scheme is considered in which a set of squeezed modes $\vec{a}^{\,m\rm squ}$ are interrogated in an alternative basis $\vec{a}^{\,\rm det}$ by a set of independent homodyne detectors. These detectors implement a multimode homodyne detection (MHD) as seen in Fig.1. Appropriately, the detection modes are viewed as resulting from a linear transformation of the independently squeezed modes [19]:

$$\vec{a}^{\,m\rm squ} = {U_T}^{-1}\vec{a}^{\,\rm det}, \tag{10}$$

where the label "m" accounts for the possibility that the squeezing quadratures are "mixed" and not uniformly $\hat{p}$, i.e., $\vec{a}^{\,\rm squ} = \Delta_{\rm squ}\vec{a}^{\,m\rm squ}$, where $\Delta_{\rm squ}$ is a diagonal matrix that aligns the squeezing quadratures into a common direction. Hence, the MHD actualizes a change of basis. Each homodyne detection is implemented on a given quadrature by choosing the phase of the local oscillator in each detection mode, which is modeled by a diagonal matrix $\Delta_{\rm LO}$ with complex elements of unit modulus. Following detection, the acquired homodyne traces are digitally recombined in a post-processing stage, which amounts to applying a real orthogonal matrix O to the detection modes. Thus, the total transformation effectuated by the MHD plus post-processing on the input squeezed modes takes the form:

$$\vec{a}_{\rm out} = O(\vec{\theta})\Delta_{\rm LO}(\vec{\varphi})U_T\Delta^*_{\rm squ}\ \vec{a}^{\,\rm squ} \equiv U_{\rm MHD}(\vec{\theta},\vec{\varphi})\ \vec{a}^{\,\rm squ}. \tag{11}$$

This transformation contains tunable degrees of freedom, namely $\Delta_{\rm LO}(\vec{\varphi})$ and $O(\vec{\theta})$, which may be optimized so as to achieve the desired output $\vec{a}_{\rm out}$. For example, they may be chosen so that $\vec{a}_{\rm out}$ replicates the statistics corresponding to a direct cluster state measurement. Alternatively, the transformation can be customized to obtain the statistics of the readout mode following a QC on an input state. It is worth noting that this method subsumes creation of the QC resource state into the state measurement itself, which reduces the quantum depth to a value of one for the ensemble of these two stages [20, 21].

Importantly, a *post-facto* examination of arbitrary linear combinations of the collected data is entirely equivalent to a direct optical transformation of the modes according to Eq. (11) followed by their detection. This equivalence is due to the fact that the matrix O is real orthogonal and does not mix the field quadratures (i.e., $\vec{a}_{\rm out}$ commutes with $\Delta_{\rm LO}U_T\Delta^*_{\rm squ}\ \vec{a}^{\,\rm squ}$).

An illustration of this approach is again provided with the four-mode linear cluster state. For this example, the squeezed mode basis, the detection basis, and the transformation U_T specified in Eq.(10) are shown in Fig.2. This detection basis is similar to that of Ref. [15, 22] in which squeezed Hermite-Gauss modes in the frequency domain are detected in a basis consisting of slices of the spectrum. The squeezing levels are taken to have the same values as in the previous demonstration. The statistics of a given quadrature of the cluster state are obtained by optimizing O and $\Delta_{\rm LO}$ to minimize the function (2), and the resultant nullifiers are listed in Table I. Each value corresponds to field fluctuations below the SN limit, which indicates successful creation of the cluster state [35]. Importantly, the nullifiers of this state can not be directly assessed with a single choice of O and

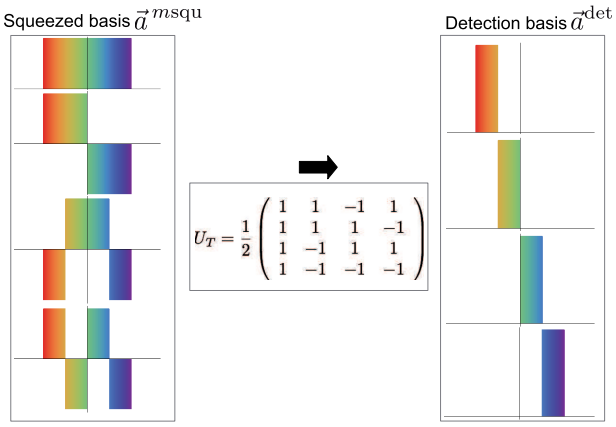

FIG. 2: Basis transformation between the squeezed modes and the MHD detection basis.

Δ_{LO} since the phase degree of freedom Δ_{LO} has been exploited to create the state itself. However, a common quadrature of all cluster nodes may be measured instead.

This strategy is also directly applicable to quantum computation. Toward that end, the primary conceptual advance taken in this work envisions the measurement of a final mode's state - the QC result - as an outcome of Eq.(4) with $U = U_{\mathrm{MHD}}$ in Eq.(1). Consequently, it is possible to make no formal assumptions as to the structure of U_{MHD} and instead directly minimize Eq.(5) (and possibly (6)) on O and Δ_{LO}; in particular, U_{MHD} may not be related to any cluster state matrix. The emphasis on the measurement outcome, rather than the building block operations necessary to achieve it, represents a new approach, which we shall refer to as "direct MBQC". It is important to stress the conceptual difference between this approach and that of Ref. [17]. Namely, effort was directed in [17] toward selecting a U_{MHD} that matches a target U_{comp}. In contrast, the present work is outcome-oriented and takes U_{MHD} to be that which minimizes Eq.(5) with no concern for its specific structure.

For the purpose of MBQC, the only pertinent matrices O are those that mix the readout mode (i.e., the mode that encodes the result) with the others. Other rotation matrices would only affect the non-symplectic part of Eqs.(3) and (4) (i.e. the displacements $\sum_{i=1}^{N-1} l_{xi} p'_i$ and $\sum_{i=1}^{N-1} l_{p_i} p'_i$). Hence, the optimization employs $2N-1$ degrees of freedom (including the N detection phases $\vec{\varphi}$ of Δ_{LO}). As an example, the Fourier transform of an input single-mode state assisted by three squeezed modes is again considered, which dictates that the coefficients of Eq.(3) are taken as $e_{\mathrm{res}} = 1$, $j_{\mathrm{res}} = -1$, $k_{\mathrm{res}} = 0$, $d_{\mathrm{res}} = 0$. A minimization of Eq.(3), which takes the squeezing levels already considered, yields the output mode:

$$\begin{aligned} \hat{x}_{\mathrm{out}} &= -1.\,\hat{p}_{\mathrm{in}} + 0.2\,\hat{p}_1^{\mathrm{squ}} - 0.97\hat{p}_2^{\mathrm{squ}} - 0.14\hat{p}_3^{\mathrm{squ}} \quad (12) \\ &\quad -0.82{p'}_1 - 0.57{p'}_2 - 0.03{p'}_{\mathrm{in}} \\ \hat{p}_{\mathrm{out}} &= 1.\,\hat{x}_{\mathrm{in}} - 0.4\hat{p}_1^{\mathrm{squ}} - 0.34\hat{p}_2^{\mathrm{squ}} + 0.54\hat{p}_3^{\mathrm{squ}} \quad (13) \\ &\quad +0.10{p'}_1 - 0.47{p'}_2 + 0.58{p'}_{\mathrm{in}}. \end{aligned}$$

Note that an outcome of this measurement provides only the $\hat{p}$ quadrature, and a scan of the global LO phase would reveal the conjugate $\hat{x}$ quadrature. On doing so, we find the values of $\Delta^2\hat{x}_{\mathrm{extra}}$ and $\Delta^2\hat{p}_{\mathrm{extra}}$ reported in Table II, which correspond to a $\sim 74\%$ reduction in the excess noise as compared to that arising from application of U_{comp}. This reduction of noise relative to the traditional approach comes at the expense of having, in principle, an approximate solution; however, in the considered example, the solution is practically exact, i.e. it exhibits an error on the order of the numerical precision of the machine used for the optimization (one part in 10^{16}).

It is interesting to consider whether the structure of the optimal U_{MHD} reproduces that of a particular U_{comp} in Eq.(8) (i.e., it may be decomposed in terms of a teleportation onto a cluster by a beam-splitter interaction, followed by successive measurements). The matrix distances between $U_{\mathrm{MHD}}^{\mathrm{best}}$ and a series of potential U_{comp} are examined; however, it does not prove feasible to discover a U_{comp} that approaches $U_{\mathrm{MHD}}^{\mathrm{best}}$ [36]. Consequently, the discovered U_{MHD} can not be interpreted as a traditional cluster-based MBQC.

The digital post-processing currently proposed may find utility in a variety of experimental situations; data acquired from multiple homodyne devices may be analyzed in a manner that reveals information regarding specific mode combinations as if those combinations had been directly measured [13]. For instance, in the experiment of Ref.[9], it is possible to reveal multiple clusters with a single optical design and the appropriate post-processing. Specifically, the matrix U_T is taken as the usual transformation converting squeezed inputs into a four-node linear cluster state (Eq.(2) of Ref.[9]) and $\Delta_{\mathrm{squ}} = \mathcal{I}$ (all of the modes are squeezed on $\hat{p}$ as in Ref.[9]). Taken alone, this unitary creates the linear cluster as in the original study. However, with an optimal choice of O and Δ_{LO}, it is also possible to construct a T-cluster $\{\frac{\Delta^2\delta_i}{\Delta^2\delta_{i_0}}\} = \{0.26, 0.27, 0.27, 0.28\}$ and a square cluster $\{0.25, 0.25, 0.26, 0.27\}$ [37].

The power of this software-based method lies in its versatility and reconfigurability. A variety of clusters or QCs may be addressed by only updating the composition of O and Δ_{LO}, as opposed to a hardware reorganization of the underlying photonic architecture. Conversely, the interest in constructing a traditional quantum network without the inclusion of supplemental post-processing is that measurements of the resultant cluster may be implemented in any quadrature. A limitation of the software

approach is indeed the necessity to update the optimized mode transformation for every variation of the detected quadrature. Nonetheless, a global scan of the local oscillator phase enables accessing both quadratures of a QC output mode or of cluster modes.

In conclusion, we have demonstrated the use of optimization strategies to mitigate noise in MBQC that arises from finite squeezing. Within the traditional cluster-based framework, the transformation between the input squeezed modes and the desired network possesses several tunable degrees of freedom, which may be optimized in order to reduce the state's excess noise. Additionally, an original approach to MBQC was proposed that does not explicitly rely on the use of cluster states. In this method, targeting the desired result of a QC and reducing the associated error due to finite squeezing are achieved by directly tuning the accessible degrees of freedom related to the detection of the resource modes. These strategies are readily implementable and open the way for increasingly compact MBQC protocols. Similar protocols for noise reduction have likewise been discussed in the context of dual rail encoding [23]. All of these schemes still remain within the domain of Gaussian transformations, and the inclusion of a non-Gaussian operation will prove necessary in order to provide an advantage with respect to classical computing [24].

This work is supported by the European Research Council starting grant Frecquam and the French National Research Agency project Comb. C.F. is a member of the Institut Universitaire de France. J.R. acknowledges support from the European Commission through Marie Curie Actions, and Y.C. recognizes the China Scholarship Council.

[1] H. J. Briegel and R. Raussendorf, Phys. Rev. Lett. **86**, 910 (2001).
[2] R. Raussendorf and H. J. Briegel, Phys. Rev. Lett. **86**, 5188 (2001).
[3] S. Yokoyama, R. Ukai, S. C. Armstrong, C. Sornphiphatphong, T. Kaji, S. Suzuki, J.-i. Yoshikawa, H. Yonezawa, N. C. Menicucci, and A. Furusawa, Nature Photonics **7**, 982 (2013).
[4] M. Chen, N. C. Menicucci, and O. Pfister, Phys. Rev. Lett. **112**, 120505 (2014).
[5] N. C. Menicucci, P. van Loock, M. Gu, C. Weedbrook, T. C. Ralph, and M. A. Nielsen, Phys. Rev. Lett. **97**, 110501 (2006).
[6] M. Gu, C. Weedbrook, N. C. Menicucci, T. C. Ralph, and P. van Loock, Phys. Rev. A **79**, 062318 (2009).
[7] N. C. Menicucci, Phys. Rev. Lett. **112**, 120504 (2014).
[8] P. van Loock, C. Weedbrook, and M. Gu, Phys. Rev. A **76**, 032321 (2007).
[9] M. Yukawa, R. Ukai, P. van Loock, and A. Furusawa, Phys. Rev. A **78**, 012301 (2008).
[10] X. Su, A. Tan, X. Jia, J. Zhang, C. Xie, and K. Peng, Phys. Rev. Lett **98**, 070502 (2007).
[11] R. Ukai, N. Iwata, Y. Shimokawa, S. C. Armstrong, A. Politi, J.-i. Yoshikawa, P. van Loock, and A. Furusawa, Phys. Rev. Lett. **106**, 240504 (2011).
[12] X. Su, Y. Zhao, S. Hao, X. Jia, C. Xie, and K. Peng, Opt. Lett **37**, 5178 (2012).
[13] G. F. et al, Supplementary Informations (????).
[14] J. Roslund, O. M. Shir, T. Bäck, and H. Rabitz, Physical Review A **80**, 043415 (2009).
[15] R. M. de Araújo, J. Roslund, Y. Cai, G. Ferrini, C. Fabre, and N. Treps, Phys. Rev. A **89**, 053828 (2014).
[16] R. Ukai, J. Yoshikawa, N. Iwata, P. van Loock, and A. Furusawa, Phys. Rev. A **81**, 032315 (2010).
[17] G. Ferrini, J. P. Gazeau, T. Coudreau, C. Fabre, and N. Treps, New J. Phys. **15**, 093015 (2013).
[18] A. Furusawa and P. V. Loock, *Quantum Teleportation and Entanglement* (Wiley-Vch, Weinheim, 2011).
[19] S. L. Braunstein, Phys. Rev. A **71**, 055801 (2005).
[20] A. Broadbent and E. Kashefi, quant-ph/0704.1736 (2007).
[21] K. E. Browne, D. E. and S. Perdrix, Proceeding of the Fifth Conference on the Theory of Quantum Computation, Communication and Cryptography (2007).
[22] J. Roslund, R. Medeiros de Araújo, S. Jiang, C. Fabre, and N. Treps, Nature Photonics **8**, 109 (2014).
[23] R. Alexander and N. C. Menicucci, arXiv:1311.3538 (2014).
[24] A. Mari and J. Eisert, Phys. Rev. Lett. **109**, 230503 (2012).
[25] N. C. Menicucci, S. T. Flammia, and P. van Loock, Physical Review A **83**, 042335 (2011).
[26] O. Pinel, P. Jian, R. M. de Araújo, J. Feng, B. Chalopin, C. Fabre, and N. Treps, Phys. Rev. Lett. **108**, 083601 (2012).
[27] G. Patera, N. Treps, C. Fabre, and G. J. de Valcarcel, Eur. Phys. J. D **56**, 123 (2010).
[28] G. Patera, C. Navarrete-Benlloch, G. J. de Valcarcel, and C. Fabre, European Physical Journal D **66** (2012).
[29] M. Beck, Phys. Rev. Lett. **84**, 5748 (2000).
[30] S. Armstrong, J.-F. Morizur, J. Janousek, B. Hage, N. Treps, P. K. Lam, and H.-A. Bachor, Nature Commun. **3**, 1026 (2012).
[31] We obtain similar results by defining $\tilde{f}_1 = \text{Mean}\left[\left\{\frac{\Delta^2\delta_i}{\Delta^2\delta_{i0}}\right\}\right]$.
[32] Other choices are once again possible, e.g. one may minimize the noise of a single quadrature only. This may be useful depending upon the specific output mode readout.
[33] An optimization following this spirit is performed analytically in Ref. [25] in a different context, with respect to local phase shifts only.
[34] As opposed to the output modes of Eq.(41), the extra noise modes are not constrained by the uncertainty principle $\Delta^2\hat{x}\Delta^2\hat{p} \geq 1$ as they are added contributions, and can display $\Delta^2\hat{x}_{\text{extra}} + \Delta^2\hat{p}_{\text{extra}} = 0$ in the limit of high squeezing. The SN limit yields $\Delta^2\hat{x}_{\text{extra}} = 3$ and $\Delta^2\hat{x}_{\text{extra}} = 2$, i.e. $\Delta^2\hat{x}_{\text{extra}} + \Delta^2\hat{p}_{\text{extra}} = 5$.
[35] The value of f_1 is larger here than the one obtained by optimization of the harder network since the full unitary group is not spanned by $O\Delta$. In principle, there is no guarantee that a solution exists for a U_{MHD} that is capable of reaching the desired target.
[36] The distance $\text{Norm}_F\left[U_V(\vec{\theta}) - U_{\text{MHD}}^{\text{best}}\right]$ is used as a metric of matrix similarity, where $\text{Norm}_F[A] = \sqrt{\Sigma_{i,j}|A_{i,j}|^2}$

is the Frobenius norm. Even upon using a free readout angle $D^{(4,4)}_{\text{meas}}$, we find a minimal norm $\text{Norm}_F \simeq 2.01$. For comparison, when U_{MHD} matches a given matrix, Norm_F amounts to the machine numerical error ($\simeq 10^{-16}$).

[37] For the linear cluster we obtain $\{0.57, 0.25, 0.25, 0.55\}$, which is better than in the original experiment as we have taken a pure state realization. The squeezing values are chosen as the minimum (5.5dB) and maximum (6.3dB) levels provided in Ref.[9] with a linear interpolation for the remaining two.

Supplementary information

Derivation of the linear optics network yielding a cluster state

In this appendix we derive Eq.(7) of the main text. First, we recall the derivation of Eq.(17) of Ref. [8], which provides a recipe allowing to compute the linear optics network corresponding to a certain cluster state. Then we provide an explicit and analytic expression for this linear optics network using the notations of Ref. [25].

Derivation of Eq.(17) in Ref. [8]

It has been shown in Ref. [8] that a cluster state with adjacency matrix V is obtained transforming the input squeezed modes as in Eq.(1) provided one choses $U = U_V = X + iY$, with

$$Y - VX = 0. \tag{14}$$

Then, in the limit of infinite squeezing the graph of the state expressed by (1) coincides with V. Here we derive Eq.(14), which coincides with Eq.(17) in Ref. [8], but expressed in the notations of Ref. [25]. The physical origin of Eq.(14) resides in the requirement that the quadrature variances of the nullifiers

$$\hat{\delta}_i \equiv \left(\hat{p}_i^C - \sum_l V_{il} \hat{x}_l^C \right) \quad \forall\, i = 1, ..., N, \tag{15}$$

tend to zero when squeezing tends to infinite. For this to hold, the coefficients multiplying the anti-squeezed quadratures terms must exactly cancel [8]. Consider a set of vacuum modes, with quadrature operators $(\vec{x}^{(0)}, \vec{p}^{(0)})^T = (\hat{x}_1^{(0)}, ..., \hat{x}_N^{(0)}, \hat{p}_1^{(0)}, ..., \hat{p}_N^{(0)})^T$. The transformations Eq.(1) as well as the initial squeezing operation can be described by means of the symplectic matrices

$$\begin{aligned} \begin{pmatrix} \vec{x}' \\ \vec{p}' \end{pmatrix} &= \begin{pmatrix} X_V & -Y_V \\ Y_V & X_V \end{pmatrix} \begin{pmatrix} K^{-\frac{1}{2}} & 0 \\ 0 & K^{\frac{1}{2}} \end{pmatrix} \begin{pmatrix} \vec{x}^{(0)} \\ \vec{p}^{(0)} \end{pmatrix} \\ &= \begin{pmatrix} X_V K^{-\frac{1}{2}} \vec{x}^{(0)} - Y_V K^{\frac{1}{2}} \vec{p}^{(0)} \\ Y_V K^{-\frac{1}{2}} \vec{x}^{(0)} + X_V K^{\frac{1}{2}} \vec{p}^{(0)} \end{pmatrix}, \end{aligned} \tag{16}$$

where we have here explicited that $\begin{pmatrix} \vec{x}^{\,\mathrm{squ}} \\ \vec{p}^{\,\mathrm{squ}} \end{pmatrix} = \begin{pmatrix} K^{-\frac{1}{2}} & 0 \\ 0 & K^{\frac{1}{2}} \end{pmatrix} \begin{pmatrix} \vec{x}^{(0)} \\ \vec{p}^{(0)} \end{pmatrix}$, K being the diagonal matrix representing the squeezing operation on each mode. In the simplest case of a uniform squeezing distribution $K = e^{-2r}\mathcal{I}$ with r real and positive, assuming that all the modes are $\hat{p}$-squeezed (the argument developed below is the same for a non-uniform squeezing distribution). When building a cluster state with graph V, we want that the quadratures transformed according to Eq.(16) satisfy approximatively $\Delta^2 \delta_i \to 0\, \forall i$, with $\hat{\delta}_i$ given in Eq.(15). In order to do so, we have to impose that the terms proportional to e^r (i.e. to $K^{-\frac{1}{2}}$) are multiplied by zero exactly. We obtain

$$\vec{p}^{\,\prime} - V\vec{x}^{\,\prime} = (Y_V K^{-\frac{1}{2}} \vec{x}^{(0)} + X_V K^{\frac{1}{2}} \vec{p}^{(0)}) - V(X_V K^{-\frac{1}{2}} \vec{x}^{(0)} - Y_V K^{\frac{1}{2}} \vec{p}^{(0)}) \to 0 \tag{17}$$

which leads to

$$\begin{aligned} &(Y_V - VX_V) K^{-\frac{1}{2}} \vec{x}^{(0)} = 0 \quad \Rightarrow \quad (Y_V - VX_V) = 0; \\ &(X_V + VY_V) K^{\frac{1}{2}} \vec{p}^{(0)} \to 0 \end{aligned} \tag{18}$$

As mentioned, the first line in Eq.(18) gives a physical meaning to the condition in Eq.(14) which allows to determine the unitary matrix U_V which generates the cluster state with graph V. The remaining "excess noise" quadratures in the second line provide variances

$$\Delta^2 \hat{\delta}_i = \left[(X_V + VY_V) \mathcal{O} K \mathcal{O}^T (X_V + VY_V)^T \right]_{ii} \tag{19}$$

which tend to zero in the infinite squeezing limit.

Derivation of the general unitary transformation associated with a cluster state Eq.(7)

We now turn to the derivation of the explicit expression Eq.(7), i.e. we seek for an explicit analytical expression for the general unitary transformation satisfying Eq.(14). This can be derived by observing that the corresponding matrix in the quadrature representation, acting on the vector $(\vec{x},\vec{p})^T$ must satisfy the requirements of symplecticity

$$XX^T + YY^T = \mathcal{I} \tag{20}$$
$$XY^T = YX^T. \tag{21}$$

Substituting Eq.(14) in Eq.(20) one obtains

$$XX^T + VXX^TV = \mathcal{I}. \tag{22}$$

Now from Eq.(21) we have

$$XX^TV = VXX^T, \tag{23}$$

which substituted in Eq.(22) gives $XX^T = (V^2 + I)^{-1}$. Hence, the symmetric solution $X_s = X_s^T$ is simply given by

$$X_s = (V^2 + I)^{-1/2} \tag{24}$$

from which, using Eq.(14), one obtains that $Y_s = V(V^2 + I)^{-1/2}$ and hence

$$U_{V\,s} = (1 + iV)(V^2 + I)^{-1/2}. \tag{25}$$

Eq.(25) represents the symmetric solution $U_{V\,s} = {U_V}_s^T$ for the linear network we were seeking for. Finally, notice that if X and Y satisfy Eq.(14), then also $X = X_s\mathcal{O}$ and $Y = Y_s\mathcal{O}$ are a solution for any real orthogonal matrix $\mathcal{O}$ due to the symmetry of Eq.(23). Hence, the general solution for the unitary matrix yielding a cluster state with graph V is provided by Eq.(7) in the main text, where we have discarded the subscript "s".

Parameterization of the most general orthogonal (angles definition)

In order to parameterize the most general element of the rotation group we use the Tait-Bryan parameterization, i.e. in dimension $N = 3$

$$\mathcal{O}(\theta_1,\theta_2,\theta_3) = \tag{26}$$
$$\begin{pmatrix} \cos\theta_1 & \sin\theta_1 & 0 \\ -\sin\theta_1 & \cos\theta_1 & 0 \\ 0 & 0 & 1 \end{pmatrix} \begin{pmatrix} \cos\theta_2 & 0 & \sin\theta_2 \\ 0 & 1 & 0 \\ -\sin\theta_2 & 0 & \cos\theta_2 \end{pmatrix} \begin{pmatrix} \cos\theta_3 & \sin\theta_3 & 0 \\ -\sin\theta_3 & \cos\theta_3 & 0 \\ 0 & 0 & 1 \end{pmatrix}.$$

In $N = 4$ we obtain the parameterization

$$\mathcal{O}(\theta_1,\theta_2,\theta_3,\theta_4,\theta_5,\theta_6) =$$
$$\begin{pmatrix} \cos\theta_1 & -\sin\theta_1 & 0 & 0 \\ \sin\theta_1 & \cos\theta_1 & 0 & 0 \\ 0 & 0 & 1 & 0 \\ 0 & 0 & 0 & 1 \end{pmatrix} \begin{pmatrix} \cos\theta_2 & 0 & -\sin\theta_2 & 0 \\ 0 & 1 & 0 & 0 \\ \sin\theta_2 & 0 & \cos\theta_2 & 0 \\ 0 & 0 & 0 & 1 \end{pmatrix} \begin{pmatrix} \cos\theta_3 & 0 & 0 & -\sin\theta_3 \\ 0 & 1 & 0 & 0 \\ 0 & 0 & 1 & 0 \\ \sin\theta_3 & 0 & 0 & \cos\theta_3 \end{pmatrix}$$
$$\begin{pmatrix} 1 & 0 & 0 & 0 \\ 0 & \cos\theta_4 & -\sin\theta_4 & 0 \\ 0 & \sin\theta_4 & \cos\theta_4 & 0 \\ 0 & 0 & 0 & 1 \end{pmatrix} \begin{pmatrix} 1 & 0 & 0 & 0 \\ 0 & \cos\theta_5 & 0 & -\sin\theta_5 \\ 0 & 0 & 1 & 0 \\ 0 & \sin\theta_5 & 0 & \cos\theta_5 \end{pmatrix} \begin{pmatrix} 1 & 0 & 0 & 0 \\ 0 & 1 & 0 & 0 \\ 0 & 0 & \cos\theta_6 & -\sin\theta_6 \\ 0 & 0 & \sin\theta_6 & \cos\theta_6 \end{pmatrix}. \tag{27}$$

In dimension $N = 6$ (relevant for some examples reported below) it is too space consuming to report all the 15 generators. To fix the convention and unambiguosly allow the reader to identify the orthogonal matrix corresponding to the solutions reported, we take the generators ordered as they come out of the sequence of Mathematica commands

```
SO[n_] := Map[RotationMatrix[\[Theta], #] &,
Subsets[Table[UnitVector[n, i], {i, n}], {2}]];  Map[ MatrixForm, SO[6]]
```

The most general $SO(6)$ element $\mathcal{O}(\theta_1,...,\theta_{15})$ is then obtained by multiplying all the resulting generators.

Generalized scheme for MBQC

Consider the very general scheme in which to the input state to be processed, plus the ancillary independent squeezed states $(\hat{a}_{\rm in}, \vec{a}^{\rm squ})$ we apply the general unitary transformation provided in Eq.(1). In order to achieve the most-general single-mode symplectic operation that can be performed on a single-mode input state, 4 ancillary squeezed modes are in principle needed (in the traditional cluster based approach). However, for the most part of single mode operations 3 ancilla modes are sufficient (this is the case for the example of the Fourier transform considered in the main text), and we stick here to the three mode case for the presentation of our strategy. The generalization to the 4-mode case is straightforward. Expliciting the vectorial structure of Eq.(1) gives

$$\begin{pmatrix} \hat{a}_{\rm in}^{'} \\ \hat{a}_1^{'} \\ \hat{a}_2^{'} \\ \hat{a}_3^{'} \end{pmatrix} = U \begin{pmatrix} \hat{a}_{\rm in} \\ \hat{a}_1^{\rm squ} \\ \hat{a}_2^{\rm squ} \\ \hat{a}_3^{\rm squ} \end{pmatrix}. \tag{28}$$

Then in the quadrature representation we can write

$$\begin{cases} \hat{x}'_{\rm in} &= f_{{\rm in},x}(\hat{x}_{\rm in}, \hat{x}_1^{\rm squ}, \hat{x}_2^{\rm squ}, \hat{x}_3^{\rm squ}, \hat{p}_{\rm in}, \hat{p}_1^{\rm squ}, \hat{p}_2^{\rm squ}, \hat{p}_4^{\rm squ}) \\ \hat{x}'_1 &= f_{1,x}(\hat{x}_{\rm in}, \hat{x}_1^{\rm squ}, \hat{x}_2^{\rm squ}, \hat{x}_3^{\rm squ}, \hat{p}_{\rm in}, \hat{p}_1^{\rm squ}, \hat{p}_2^{\rm squ}, \hat{p}_4^{\rm squ}) \\ \hat{x}'_2 &= f_{2,x}(\hat{x}_{\rm in}, \hat{x}_1^{\rm squ}, \hat{x}_2^{\rm squ}, \hat{x}_3^{\rm squ}, \hat{p}_{\rm in}, \hat{p}_1^{\rm squ}, \hat{p}_2^{\rm squ}, \hat{p}_4^{\rm squ}) \\ \hat{x}'_3 &= f_{3,x}(\hat{x}_{\rm in}, \hat{x}_1^{\rm squ}, \hat{x}_2^{\rm squ}, \hat{x}_3^{\rm squ}, \hat{p}_{\rm in}, \hat{p}_1^{\rm squ}, \hat{p}_2^{\rm squ}, \hat{p}_4^{\rm squ}) \end{cases} \tag{29}$$

and

$$\begin{cases} \hat{p}'_{\rm in} &= f_{{\rm in},p}(\hat{x}_{\rm in}, \hat{x}_1^{\rm squ}, \hat{x}_2^{\rm squ}, \hat{x}_3^{\rm squ}, \hat{p}_{\rm in}, \hat{p}_1^{\rm squ}, \hat{p}_2^{\rm squ}, \hat{p}_4^{\rm squ}) \\ \hat{p}'_1 &= f_{1,p}(\hat{x}_{\rm in}, \hat{x}_1^{\rm squ}, \hat{x}_2^{\rm squ}, \hat{x}_3^{\rm squ}, \hat{p}_{\rm in}, \hat{p}_1^{\rm squ}, \hat{p}_2^{\rm squ}, \hat{p}_4^{\rm squ}) \\ \hat{p}'_2 &= f_{2,p}(\hat{x}_{\rm in}, \hat{x}_1^{\rm squ}, \hat{x}_2^{\rm squ}, \hat{x}_3^{\rm squ}, \hat{p}_{\rm in}, \hat{p}_1^{\rm squ}, \hat{p}_2^{\rm squ}, \hat{p}_4^{\rm squ}) \\ \hat{p}'_3 &= f_{3,p}(\hat{x}_{\rm in}, \hat{x}_1^{\rm squ}, \hat{x}_2^{\rm squ}, \hat{x}_3^{\rm squ}, \hat{p}_{\rm in}, \hat{p}_1^{\rm squ}, \hat{p}_2^{\rm squ}, \hat{p}_4^{\rm squ}) \end{cases}, \tag{30}$$

where the functions $f_{i,x}, f_{i,p}$ $(i = 1, 2, 3)$, $f_{{\rm in},x}, f_{{\rm in},p}$ depend on the applied transformation U.

Suppose now the quadrature $\hat{p}$ is measured on all the modes, except the last one, which represents the result of the computation, and which measurement constitutes the readout. In the Heisenberg representation, the projective measurement of $\hat{p}'_{\rm in}, \hat{p}'_1, \hat{p}'_2$ effectively results in replacing these operators by the corresponding measurement outcomes $p'_{\rm in}$, p'_1 and p'_2 in Eq.(36), which are real numbers [18]. Then, the linear system composed of the first 3 lines in Eq.(30) is solved for the anti-squeezed observables $\hat{x}_1^{\rm squ}, \hat{x}_2^{\rm squ}, \hat{x}_3^{\rm squ}$. These are then replaced in the last line of Eqs.(29) and (30), i.e. in the expression of the output mode variables $\hat{p}'_3, \hat{x}'_3$, yielding the result in Eq.(3). This very general scheme encompasses both the traditional MBQC scheme based on cluster states, as well as the newly proposed method based on the post-processing. Examples of both paradigms are provided in the following.

Traditional measurement based quantum computation and calculation of the error on the result mode

In the traditional realization of the measurement based quantum computation scheme on a single mode input state presented above, the state to be processed is first attached to a linear cluster state via teleportation. This is implemented e.g. via a beam-splitter interaction between the mode containing the input state and the first mode of the cluster, and a subsequent measurement of the quadratures of these two modes. The right quadrature measurement ($\hat{x}_{\rm in}$, $\hat{x}_1$ with the choice of the beam splitter as in Eq.(32)) effectively projects the unalterated input state on the second mode of the cluster state, a part from displacements operators which depend on the outcomes of the measurement and which can be corrected for. Then, the second and in general third modes of the cluster state are measured on suitable quadratures, depending on the computation that we want to perform, which can be determined with the recipe of Ref. [16]. Consider the specific example of the Fourier transform discussed in the main text to fix the ideas. For the Fourier transform it turns out that a three-mode ancilla cluster is enough, and that the quadrature $\hat{p}_2$ should be measured on its second mode (as will be clear afterwards), in order to project the Fourier-transformed input state on the last mode of the cluster. Note that, as already stressed in the main text, since all the measurements here performed are gaussian, they can be done simultaneously - no adaptation of the measurement basis is effectively needed [6].

FIG. 3: A MBQC scheme where a Fourier transform is implemented on an input state by attaching it to a linear cluster state and by performing measurements on the cluster modes.

These quadrature measurements on each mode can be equivalently described as a suitable rotation matrix $D_{\rm meas}$, followed by a measurement in the same quadrature on all the modes, say, $\hat{p}$ - in other words, measuring $\hat{p}$ on the modes *in* and 1 after having rotated them by $\pi/2$ corresponds to the measure of $\hat{x}_{\rm in}$ and $\hat{x}_1$. To summarize, starting from the input mode and a collection of three $\hat{p}$-squeezed modes, the sequence of matrices to implement a Fourier transform when measuring the $\hat{p}$ quadrature on every mode consists in a first matrix leading to the three component cluster state $U_{\rm clu}^{1,2,3}$, followed by a beam-splitter interaction between the first cluster mode and the input mode $U_{\rm BS}^{\rm in,1}$, and by a rotation matrix which tells which quadrature is measured on each mode $D_{\rm meas}$ [11, 16, 17], i.e.

$$\begin{pmatrix} \hat{a}_{\rm in}^{'} \\ \hat{a}_1^{'} \\ \hat{a}_2^{'} \\ \hat{a}_3^{'} \end{pmatrix} = D_{\rm meas} U_{\rm BS}^{\rm in,1} U_{\rm clu}^{1,2,3} \begin{pmatrix} \hat{a}_{\rm in} \\ \hat{a}_1^{\rm squ} \\ \hat{a}_2^{\rm squ} \\ \hat{a}_3^{\rm squ} \end{pmatrix} \equiv U_{\rm comp} \begin{pmatrix} \hat{a}_{\rm in} \\ \hat{a}_1^{\rm squ} \\ \hat{a}_2^{\rm squ} \\ \hat{a}_3^{\rm squ} \end{pmatrix}. \tag{31}$$

Fixed realization of the cluster matrix

For instance, let us consider first the case in which we chose as the matrix building the cluster state from independently squeezed modes Eq.(7) the realization given in Ref.[17]. Then the matrices defining a Fourier transform quantum computation which appear in Eq.(31) are given by

$$D_{\rm meas} = {\rm diag}(i,i,1,1); \tag{32}$$

$$U_{\rm BS}^{\rm in,1} = \begin{pmatrix} \frac{1}{\sqrt{2}} & \frac{i}{\sqrt{2}} & 0 & 0 \\ \frac{i}{\sqrt{2}} & \frac{1}{\sqrt{2}} & 0 & 0 \\ 0 & 0 & 1 & 0 \\ 0 & 0 & 0 & 1 \end{pmatrix}; U_{\rm clu}^{1,2,3} = \begin{pmatrix} 1 & 0 & 0 & 0 \\ 0 & 0 & -\sqrt{\frac{2}{3}} & -\frac{i}{\sqrt{3}} \\ 0 & -\frac{i}{\sqrt{2}} & -\frac{i}{\sqrt{6}} & -\frac{1}{\sqrt{3}} \\ 0 & -\frac{1}{\sqrt{2}} & \frac{1}{\sqrt{6}} & -\frac{i}{\sqrt{3}} \end{pmatrix}$$

from which

$$U_{\rm comp} = D_{\rm meas} U_{\rm BS}^{\rm in,1} U_{\rm clu}^{1,2,3} = \begin{pmatrix} \frac{i}{\sqrt{2}} & 0 & \frac{1}{\sqrt{3}} & \frac{i}{\sqrt{6}} \\ -\frac{1}{\sqrt{2}} & 0 & -\frac{i}{\sqrt{3}} & \frac{1}{\sqrt{6}} \\ 0 & -\frac{i}{\sqrt{2}} & -\frac{i}{\sqrt{6}} & -\frac{1}{\sqrt{3}} \\ 0 & -\frac{1}{\sqrt{2}} & \frac{1}{\sqrt{6}} & -\frac{i}{\sqrt{3}} \end{pmatrix}. \tag{33}$$

The squeezed input mode can be related to vacua modes as follows:

$$\begin{pmatrix} \vec{x}^{\rm squ} \\ \vec{p}^{\rm squ} \end{pmatrix} = \begin{pmatrix} K^{-\frac{1}{2}} & 0 \\ 0 & K^{\frac{1}{2}} \end{pmatrix} \begin{pmatrix} \vec{x}^{(0)} \\ \vec{p}^{(0)} \end{pmatrix} \tag{34}$$

with $K^{-\frac{1}{2}} = {\rm diag}(1, e^{r_1}, e^{r_2}, e^{r_3})$ and $\vec{x}^{(0)} = (x_{\rm in}^{(0)}, x_1^{(0)}, x_2^{(0)}, x_3^{(0)})^T$. By direct application of the transformation defined by Eq.(31) in the quadrature representation we obtain the quadratures of the transformed modes which are given by

$$\begin{cases} \hat{x}'_{\rm in} = -\frac{\hat{p}_3^{\rm squ}}{\sqrt{6}} - \frac{\hat{p}_{\rm in}}{\sqrt{2}} + \frac{\hat{x}_2^{\rm squ}}{\sqrt{3}} \\ \hat{x}'_1 = \frac{\hat{p}_2^{\rm squ}}{\sqrt{3}} + \frac{\hat{x}_3^{\rm squ}}{\sqrt{6}} - \frac{\rm xin}{\sqrt{2}} \\ \hat{x}'_2 = \frac{\hat{p}_1^{\rm squ}}{\sqrt{2}} + \frac{\hat{p}_2^{\rm squ}}{\sqrt{6}} - \frac{\hat{x}_3^{\rm squ}}{\sqrt{3}} \\ \hat{x}'_3 = \frac{\hat{p}_3^{\rm squ}}{\sqrt{3}} - \frac{\hat{x}_1^{\rm squ}}{\sqrt{2}} + \frac{\hat{x}_2^{\rm squ}}{\sqrt{6}}. \end{cases} \tag{35}$$

and by

$$\left\{\begin{array}{rcll} \hat{p}'_{\rm in} &=& \frac{\hat{p}_2^{\rm squ}}{\sqrt{3}}+\frac{\hat{x}_3^{\rm squ}}{\sqrt{6}}+\frac{\hat{x}_{\rm in}}{\sqrt{2}} & a) \\ \hat{p}'_1 &=& \frac{\hat{p}_3^{\rm squ}}{\sqrt{6}}-\frac{\hat{p}_{\rm in}}{\sqrt{2}}-\frac{\hat{x}_2^{\rm squ}}{\sqrt{3}} & b) \\ \hat{p}'_2 &=& -\frac{\hat{p}_3^{\rm squ}}{\sqrt{3}}-\frac{\hat{x}_1^{\rm squ}}{\sqrt{2}}-\frac{\hat{x}_2^{\rm squ}}{\sqrt{6}} & c) \\ \hat{p}'_3 &=& -\frac{\hat{p}_1^{\rm squ}}{\sqrt{2}}+\frac{\hat{p}_2^{\rm squ}}{\sqrt{6}}-\frac{\hat{x}_3^{\rm squ}}{\sqrt{3}}. & d) \end{array}\right. \tag{36}$$

As before, in this Heisenberg representation, the projective measurement of $\hat{p}'_{\rm in}, \hat{p}'_1, \hat{p}'_2$ effectively results in replacing these operators by the corresponding measurement outcomes $p'_{\rm in}$, p'_1 and p'_2 in Eq.(36) [18]. Then, Eqs.(36) and the last line in Eq.(35) are solved for the output mode variables $\hat{p}'_3, \hat{x}'_3$, eliminating the anti-squeezed observables $\hat{x}_1^{\rm squ}, \hat{x}_2^{\rm squ}, \hat{x}_3^{\rm squ}$. We obtain from (36-a)

$$\frac{\hat{x}_3^{\rm squ}}{\sqrt{3}} = \sqrt{2}p'_{\rm in} - \sqrt{2}\frac{\hat{p}_2^{\rm squ}}{\sqrt{3}} - \hat{x}_{\rm in}$$

which substituted in Eq. (36-d) gives

$$\hat{p}'_3 = \hat{x}_{\rm in} - \frac{\hat{p}_1^{\rm squ}}{\sqrt{2}} + 3\frac{\hat{p}_2^{\rm squ}}{\sqrt{6}} - \sqrt{2}p'_{\rm in} \tag{37}$$

From (36-b)

$$\hat{x}_2^{\rm squ} = -\sqrt{3}p'_1 + \frac{1}{\sqrt{2}}\hat{p}_3^{\rm squ} - \sqrt{\frac{3}{2}}\hat{p}_{\rm in} \tag{38}$$

while from (36-c) we have

$$\hat{x}_1^{\rm squ} = -\sqrt{2}p'_2 - \sqrt{\frac{2}{3}}\hat{p}_3^{\rm squ} - \frac{1}{\sqrt{3}}\hat{x}_2^{\rm squ} \tag{39}$$

which substituted in the equation for $\hat{x}'_3$ gives

$$\hat{x}'_3 = -\hat{p}_{\rm in} + p'_2 - \sqrt{2}p'_1 + \sqrt{3}\hat{p}_3^{\rm squ} \tag{40}$$

Identifying $\hat{x}_{\rm out} = \hat{x}'_3$ and $\hat{p}_{\rm out} = \hat{p}'_3$, from (37) and (40) and making use of Eq.(34) we obtain

$$\begin{aligned} \hat{x}_{\rm out} &= \hat{x}'_3 = -\hat{p}_{\rm in} + p'_2 - \sqrt{2}p'_1 + \sqrt{3}\hat{p}_3^{\rm squ} \\ \hat{p}_{\rm out} &= \hat{p}'_3 = \hat{x}_{\rm in} - \sqrt{2}p'_{\rm in} - \frac{\hat{p}_1^{\rm squ}}{\sqrt{2}} + 3\frac{\hat{p}_2^{\rm squ}}{\sqrt{6}}. \end{aligned} \tag{41}$$

As mentioned in the main text, the result projected on the last mode of the cluster state (see Fig. 3) is the desired Fourier transform of the input mode, plus some displacement which depends on the outcomes of the measurements performed on the previous modes (and which can be corrected by re-displacing back the last mode), as well as an undesired contribution due to the finite squeezing degree on the measured modes. The latter contributions eventually tend to zero when the squeezing degree goes to infinite in all the modes. Indeed the extra noise affecting the result associated with these undesired contributions is given by

$$\begin{aligned} \Delta^2\hat{x}_{\rm extra} &= \Delta^2\left[\sqrt{3}e^{-r_3}\hat{p}_3^{(0)}\right] = 3e^{-2r_3}\Delta_0^2 \\ \Delta^2\hat{p}_{\rm extra} &= \Delta^2\left[e^{-r_1}\frac{\hat{p}_1^{(0)}}{\sqrt{2}} + 3e^{-r_2}\frac{\hat{p}_2^{(0)}}{\sqrt{6}}\right] = \left(e^{-2r_1}+3e^{-2r_2}\right)\frac{\Delta_0^2}{2}. \end{aligned} \tag{42}$$

We can re-express the extra-noise contributions appearing in Eq.(41) in terms of the cluster nullifiers. With the definition of the matrix leading to the cluster state expressed by Eq.(32) we have

$$\vec{a}^{\rm clu} = U_{\rm clu}^{1,2,3}\vec{a}^{\rm squ} \tag{43}$$

(regarding only to the cluster modes) leading to

$$\begin{cases} \hat{x}_1^{\rm clu} &= \frac{\hat{p}_3^{\rm squ}}{\sqrt{3}} - \sqrt{\frac{2}{3}}\hat{x}_2^{\rm squ} \\ \hat{x}_2^{\rm clu} &= \frac{\hat{p}_1^{\rm squ}}{\sqrt{2}} + \frac{\hat{p}_2^{\rm squ}}{\sqrt{6}} - \frac{\hat{x}_3^{\rm squ}}{\sqrt{3}} \\ \hat{x}_3^{\rm clu} &= \frac{\hat{p}_3^{\rm squ}}{\sqrt{3}} - \frac{\hat{x}_1^{\rm squ}}{\sqrt{2}} + \frac{\hat{x}_2^{\rm squ}}{\sqrt{6}} \end{cases} \tag{44}$$

and

$$\begin{cases} \hat{p}_1^{\rm clu} &= -\sqrt{\frac{2}{3}}\hat{p}_2^{\rm squ} - \frac{\hat{x}_3^{\rm squ}}{\sqrt{3}} \\ \hat{p}_2^{\rm clu} &= -\frac{\hat{p}_3^{\rm squ}}{\sqrt{3}} - \frac{\hat{x}_1^{\rm squ}}{\sqrt{2}} - \frac{\hat{x}_2^{\rm squ}}{\sqrt{6}} \\ \hat{p}_3^{\rm clu} &= -\frac{\hat{p}_1^{\rm squ}}{\sqrt{2}} + \frac{\hat{p}_2^{\rm squ}}{\sqrt{6}} - \frac{\hat{x}_3^{\rm squ}}{\sqrt{3}}. \end{cases} \tag{45}$$

From Eqs.(44) and (45) one can compute the nullifiers

$$\begin{aligned} \hat{\delta}_1 &= \hat{p}_1^{\rm clu} - \hat{x}_2^{\rm clu} = -\frac{\hat{p}_1^{\rm squ} + \sqrt{3}\hat{p}_2^{\rm squ}}{\sqrt{2}} \\ \hat{\delta}_2 &= \hat{p}_2^{\rm clu} - \hat{x}_1^{\rm clu} - \hat{x}_3^{\rm clu} = -\sqrt{3}\hat{p}_3^{\rm squ} \\ \hat{\delta}_3 &= \hat{p}_3^{\rm clu} - \hat{x}_2^{\rm clu} = -\sqrt{2}\hat{p}_1^{\rm squ} \end{aligned} \tag{46}$$

It is then straightforward to re-express the terms of extra noise in Eqs.(41) as

$$\begin{aligned} \sqrt{3}\hat{p}_3^{\rm squ} &= -\hat{\delta}_2, \\ -\frac{\hat{p}_1^{\rm squ}}{\sqrt{2}} + 3\frac{\hat{p}_2^{\rm squ}}{\sqrt{6}} &= -\hat{\delta}_1 + \hat{\delta}_3 \end{aligned} \tag{47}$$

yielding to Eq.(9) of the main text, where $\hat{\delta}_i$ are the nullifiers defined in Eq.(15).

Optimized realization of the cluster matrix

We now run an evolutionary algorithm, which seeks to minimize Eq.(6) over the angles $\vec{\theta}$, thereby reducing as much as possible the variances of the nullifiers providing extra noise in the result of the Fourier transform. We obtain the optimized cluster matrix corresponding to the angles (in units of 2π) $\{0.8, 0.75, 0.71\}$, which yields

$$U_{\rm clu}^{1,2,3} = \begin{pmatrix} -9.8\times10^{-8} + 0.58i & 0.71 + \left(8.9\times10^{-8}\right)i & 0.41 - \left(1.5\times10^{-8}\right)i \\ 0.58 + \left(2.1\times10^{-8}\right)i & 8.9\times10^{-8} - \left(1.\times10^{-8}\right)i & -1.5\times10^{-8} + 0.82i \\ 1.2\times10^{-7} + 0.58i & -0.71 + \left(8.9\times10^{-8}\right)i & 0.41 - \left(1.5\times10^{-8}\right)i \end{pmatrix}, \tag{48}$$

from which one can easily compute the cluster modes $\vec{a}^{\rm clu} = U_{\rm clu}^{1,2,3}\vec{a}^{\rm squ}$. All the arguments presented above for the fixed realization of the cluster unitary matrix can be repeated; in particular, the output modes analogous to Eq.(41) are given by

$$\begin{aligned} \hat{x}_{\rm out} &= -\hat{p}_{\rm in} - 1.7\hat{p}_1^{\rm squ} + \left(2.4\cdot10^{-7}\right)\hat{p}_2^{\rm squ} + \left(5.5\cdot10^{-8}\right)\hat{p}_3^{\rm squ} - 1.4p_1' + p_2' \\ \hat{p}_{\rm out} &= \hat{x}_{\rm in} + \left(2.\cdot10^{-7}\right)\hat{p}_1^{\rm squ} + 1.4\hat{p}_2^{\rm squ} - \left(1.3\cdot10^{-8}\right)\hat{p}_3^{\rm squ} - 1.4p_{\rm in}' \end{aligned} \tag{49}$$

with $\hat{p}_i^{\rm squ} = e^{-r_i}\hat{p}_i^{(0)}$. Again, it is possible to recast the noise terms appearing in Eq.(49) in terms of the nullifiers, obtaining the same as in Eq.(9). As shown in the main text, the value of the nullifier variances however depends on the specific realization of the matrix used, which allows choosing Eq.(48) as the best realization, yielding the lowest nullifier variances (see main text).

Optimized cluster state generation for non-pure states: examples from our experiment

To draw specific examples of the application of our optimization methods for cluster state generation in the case of a non-pure state, we are going to use the state obtained in our experiment. This consists in a Synchronously Pumped

Optical Parametric Oscillator (SPOPO), which produces squeezed states in a suitable basis (see Refs. [15, 22, 26]). First we provide some detail about the experiment, generating independent squeezed modes. Then, we show how to evidence cluster state correlations with data collected in this experiment, first with the traditional method, requiring optimization of the cluster network matrix $U_V(\vec{\theta})$, and then with the direct approach, where we are going to optimize on the experimental parameters O, Δ_{LO} according with the discussion presented in the main text. To highlight our method, we will focus on the example of the six-mode linear cluster state.

Remindings of the SPOPO experiment

This experiment is based on the interaction of light coming from a synchronously pumped femto-second laser with a non-linear crystal in a cavity, realizing a synchronously pumped optical parametric oscillator (SPOPO). The quantum state originating from the SPOPO has been extensively characterized, both theoretically [27, 28] and experimentally [15, 22, 26]. In the SPOPO, the parametric downconversion of the pump femtosecond comb establishing correlations between the frequencies of the downconverted comb. On the basis of the "supermodes" (that are linear combinations of the original, single frequency modes, enveloped by a Hermite-Gauss profile) the system is described as a set of independently squeezed modes [15, 27]. The squeezing quadrature turns out to alternate between the $\hat{x}$ and $\hat{p}$ with increasing mode index, i.e. $\Delta^*_{\mathrm{squ}} = (i, 1, i, 1, ...)$. The full experimental reconstruction of the SPOPO state has been obtained in the "pixel" basis [15] via homodyne detection and pulse-shaping of the LO. This means that the LO spectrum has been divided into discrete bands of equal energy (the frequency "pixels"), e.g., in six bands. This has allowed to measure the noise properties in each pixel, as well as the correlations among different spectral regions. In this way, the covariance matrix has been reconstructed in the pixel basis, as explained in detail in Ref. [15]. This procedure has required repeating the homodyne detection several times. Future experimental progresses may allow assessing the noise properties of the SPOPO spectrum on all pixels simultaneously, by the use of a multi-pixel homodyne detector [29, 30].

A typical 6-mode covariance matrix measured in the pixel basis, with a 6-slice pixelization of the LO spectrum, yields

$$\Sigma^E_{qq} = \begin{pmatrix} 2.2 & 0.51 & 0.15 & -0.05 & -0.35 & -1.8 \\ 0.51 & 1.3 & 0.13 & -0.1 & -0.43 & -0.85 \\ 0.15 & 0.13 & 0.97 & -0.17 & -0.28 & -0.42 \\ -0.05 & -0.1 & -0.17 & 0.83 & -0.11 & -0.14 \\ -0.35 & -0.43 & -0.28 & -0.11 & 1.1 & 0.14 \\ -1.8 & -0.85 & -0.42 & -0.14 & 0.14 & 2.4 \end{pmatrix}$$

$$\Sigma^E_{pp} = \begin{pmatrix} 2.2 & 0.38 & 0.29 & 0.25 & 0.44 & 2. \\ 0.38 & 1.6 & 0.49 & 0.56 & 0.68 & 0.99 \\ 0.29 & 0.49 & 1.7 & 0.69 & 0.74 & 0.67 \\ 0.25 & 0.56 & 0.69 & 1.9 & 0.68 & 0.6 \\ 0.44 & 0.68 & 0.74 & 0.68 & 1.8 & 0.64 \\ 2. & 0.99 & 0.67 & 0.6 & 0.64 & 2.4 \end{pmatrix}. \quad (50)$$

Let us indicate the measured covariance matrix in the pixel basis by $\Sigma^E = \begin{pmatrix} \Sigma^E_{qq} & 0 \\ 0 & \Sigma^E_{pp} \end{pmatrix}$ (the suffix "E" stands for "experimental"). The constituent block matrices Σ^E_{qq} and Σ^E_{pp} are given in Eq.(50), where assume the convention $\Delta^2 \hat{x}_{i0} = 1$ for the vacuum fluctuations. The block structure shows that there are no correlations among the $\hat{p}$ and $\hat{x}$ quadratures.

The diagonalization of the matrices Σ^E_{qq} and Σ^E_{pp} yields here to two similar eigensystems - in the ideal case of a pure state free from experimental imperfections they would be identical. In order to derive a unique diagonalization matrix, the eigenstructures corresponding to the anti-squeezed modes, which likewise alternate between the two quadratures and which exhibit increased robustness to noise, are orthogonalized by a Gram-Schmidt procedure. This new basis approximatively diagonalizes each of the two blocks of the covariance matrix in the pixel basis, thereby providing us with the matrix U_T, which transforms the correlated pixel modes onto independent squeezed modes according to

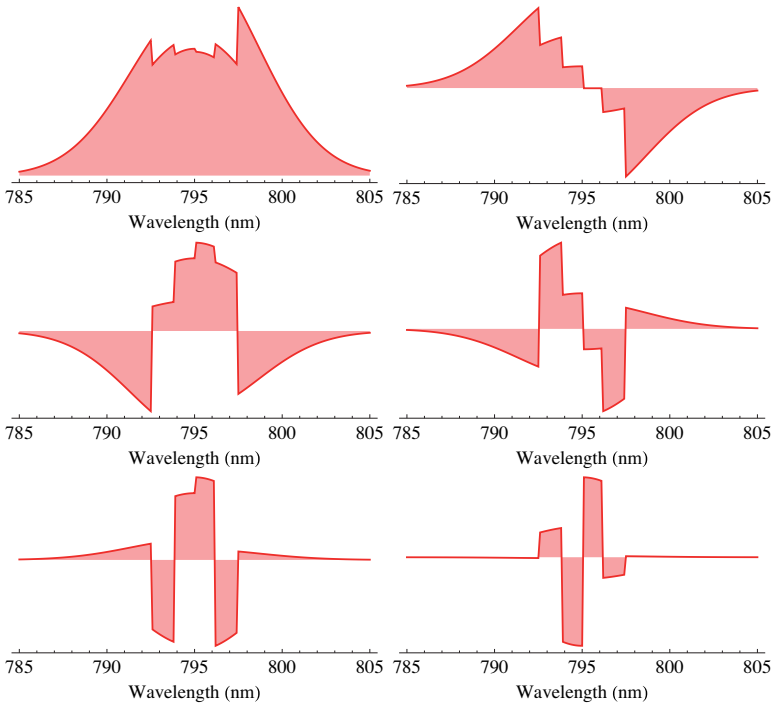

FIG. 4: Amplitude spectra corresponding to each of the orthogonal supermodes retrieved from the covariance matrix.

Eq.(10). The so retrieved supermodes are represented in Fig. 4, and these modes are squeezed according to quadratures defined by $\Delta^*_{\rm squ} = (i, 1, i, 1, i, 1)$.

Once the covariance matrix is expressed in the independently squeezed supermodes basis, we can apply to it the transformation U_V which implements the cluster state with graph V (this allows to account for a general case in which the state produced in the experiment is not pure, hence the anti-squeezing is not perfectly equal to the inverse of the squeezing). The resulting overall transformation to be applied to the covariance matrix in the pixel basis to evidence cluster correlation then reads

$$\vec{a}^C = U_V \Delta_{\rm squ} {U_T}^{-1} \vec{a}^{\rm pix} \equiv U_{\rm sol} \vec{a}^{\rm pix}. \tag{51}$$

To the unitary matrix in Eq.(51) acting on the annihilation operators corresponds the simplectic transformation to be applied on the measured covariance matrix

$$\Sigma^C = S_{\rm sol} \Sigma^E S_{\rm sol}^T, \tag{52}$$

where $S_{\rm sol} = \begin{pmatrix} X_{\rm sol} & -Y_{\rm sol} \\ Y_{\rm sol} & X_{\rm sol} \end{pmatrix}$ with $U_{\rm sol} = X_{\rm sol} + iY_{\rm sol}$. The cluster-type correlations can then be tested checking whether the combinations of quadratures expressed by Eq.(15) have variances below the shot noise. The latter limit is defined in this context as the variances which are obtained by feeding the linear network with vacua in input, instead that of squeezed states.

Since the measurements have been obtained here in the pixel basis, where each pixel measurement has required a separate shaping of the LO, obtaining cluster modes as in Eq.(51) has to be intended as a "simulation" of the cluster correlations that can be obtained and measured in our experiment.

Optimization of the "traditional" cluster state generation for the non pure SPOPO state

For example, one may consider the application of the unitary matrix which builds up a 6-mode linear cluster state. Using the symmetric realization of Eq.(25), $U_{V\,s} = {U_V}_s^T$, and applying the cluster transformation Eq.(52) to the covariance matrix in Eq.(50), we obtain the nullifier variances

$$\{\frac{\Delta^2 \delta_i}{\Delta^2 \delta_{i0}}\} = \{0.172, 0.196, 0.76, 1., 0.912, 1.16\}, \tag{53}$$

which have been normalized to the shot noise $\{\Delta^2\delta_{i0}\} = \{2, 3, 3, 3, 3, 2\}$. We see from Eq.(53) that not all the nullifier variances lie below 1, i.e. below the shot noise, and the value of f_1 in Eq.(2) is $f_1 = 1.7$.

We can compare the nullifier variances obtained in Eq.(53) with the ones obtained optimizing the cluster unitary transformation. In 6 dimensions, the Tait-Bryan parameterization analogous to Eq.(26) involves 15 angles $\vec{\theta} = (\theta_1, ..., \theta_{15})$. We use the strategy presented in the main text, targeting a minimal fitness function based on the nullifier variances as defined in Eq.(2). Performing the optimization on the angular variables $\vec{\theta}$ with the use of the evolutionary strategy the obtained optimized variances of the nullifiers are now

$$\{\frac{\Delta^2\delta_i}{\Delta^2\delta_{i0}}\} = \{0.77, 0.521, 0.344, 0.356, 0.535, 0.782\}, \tag{54}$$

corresponding to the set of angular variables (normalized to 2π)
$\vec{\theta} = \{0.219, 0.582, 0.882, 0.444, 0.539, 0.167, 0.564, 0.405, 0.47, 0.827, 0.86, 0.57, 0.63, 0.461, 0.908\}$. Compared to the variances obtained by applying the symmetric unitary matrix Eq.(25), which were reported in Eq.(53), we see that the optimized unitary network has allowed the simultaneous lowering of all the variances below the shot noise. The values of f_1 has been lowered to $f_1 = 1.2$.

"direct" cluster state optimization for the non pure SPOPO state

In order to measure the nullifier variances corresponding to a certain cluster state below the shot noise with the direct method, one can numerically minimize them over the degrees of freedom expressed by O, Δ_{LO} by applying the transformation (11) on the squeezed modes, and computing the resulting nullifiers. We will assume that the state of the system was stable enough, such that the SPOPO state reconstructed by separately measuring each pixel is the same as if all the pixels were measured at the same time with a MHD. Hence, from the experimentally measured state in the pixel basis we will draw conclusions concerning future experiments with the MHD.

We minimize the same function (2) this time on O, Δ_{LO} and obtain the nullifiers $\{\frac{\Delta^2\delta_i}{\Delta^2\delta_{i0}}\} = \{0.51, 0.697, 0.626, 0.51, 0.708, 0.496\}$, corresponding to $f_1 = 1.4$. As in the pure state example carried out in the main text, though this results in a higher f_1 than the one obtained with the optimized version of the network U_V (see paragraph above), the direct optimization has still allowed the simultaneous lowering of all the nullifiers below the shot noise.

Note however that these nullifiers cannot be measured with this choice of O, Δ_{LO}, consistently with the discussion in the main text. The same quadrature on all the cluster modes can be measured instead.